光学学报

太赫兹介质超表面实现双域多信道复用

王羚[1*]，高峰[1]，滕书华[1]，谭志国[1]，张星[1]，娄军[1]，邓力[2**]
[1]湖南第一师范学院电子信息学院，湖南 长沙 410205；
[2]北京邮电大学信息与通信工程学院，北京 100876

摘要 提出一种工作于0.25～0.35 THz的介质超表面，基于该超表面、结合轨道角动量(OAM)和频率域实现双域多信道复用，理论上可实现$4\times N$(N为任意正整数)路携带不同信息的正交同轴波束的同时传输。超表面由介质柱阵列和介质基板构成，可基于Pancharatnam-Berry相位原理进行设计。选取0.25、0.3、0.35 THz三个频点进行仿真验证，结果表明：当3路具有不同频率和入射角的圆极化平面波沿4个不同方向斜入射至超表面上时，在垂直于超表面的方向上，12路交叉极化透射波被转换为彼此拓扑正交或频率正交的同轴波束，即结合OAM和频率域实现了12路信道复用。所提出的介质超表面在高速率大容量太赫兹通信领域具有潜在的应用价值。

关键词 表面光学；太赫兹；介质超表面；复用；轨道角动量
中图分类号 O436 **文献标志码** A **DOI**: 10.3788/AOS221337

1 引 言

随着信息技术的快速发展，近年来，为实现高速率大容量无线通信系统，太赫兹(THz)频段(0.1～10 THz)引起了研究人员的极大关注，太赫兹无线通信也成为第六代移动通信的关键技术之一[1]。利用复用技术，基于空间、极化、频率(波长)、复振幅(幅度和相位)和时间5个物理维度(域)可实现多个正交信道的同时传输，如极化复用、空分复用和频分复用，从而提高无线通信数据传输速率、增大系统容量[2]。此外，同时利用两个或多个物理维度实现双域或多域复用可进一步提高系统速率、增大系统容量，具有很大的研究价值。

携带轨道角动量(OAM)的电磁波称为OAM波或涡旋波[3]。OAM波具有相位因子$\exp(\mathrm{j}l\varphi)$(其中j为虚数单位，l和φ分别为OAM波的拓扑荷和空间方位角，理论上l可取任意整数和分数，且具有不同l的OAM波相互正交)，能量呈环形分布，相位呈螺旋形分布。基于此，可将OAM作为一种新形式的信息载体，通过提供额外的维度来实现空间复用。超表面[4]作为一种二维超材料[5]，由周期或准周期亚波长单元阵列构成，在电磁波传播方向上具有超薄的厚度，通过引入突变相位可实现对电磁波幅度、相位和极化的有效控制。基于主要使用的材料类型，超表面可分成金属超表面和介质超表面两大类。此前，大部分研究集中于利用金属超表面产生OAM波束[6-9]或实现OAM波束复用[10-13]。相比于金属超表面，介质超表面[14-15]具有欧姆损耗更小、成本更低、易于加工制造、传输效率更高等优势。因此，基于介质超表面生成单个OAM波[16-17]、进一步实现OAM波束复用已成为研究热点。

目前，基于介质超表面实现OAM波束复用的方法主要有：1)基于单个介质超表面，将一路入射波转换成多路具有不同拓扑的正交OAM波[18-22]；2)基于极化复用介质超表面，将正交线极化或圆极化(CP)入射波转换成具有不同拓扑的正交OAM波[23-27]；3)基于介质超表面阵列生成多路正交OAM波[28-31]。这些方法存在OAM波携带的信息相同、可实现的复用信道数有限、通信系统的复杂性和成本较高的缺点。虽然有研究基于角度复用介质超表面，利用多路具有不同角度的入射波生成正交OAM同轴波束，实现复用[32-34]，有效解决了以上问题，然而目前的角度复用介质超表面只能工作于单频点，一旦入射波频率发生变化，生成的OAM波会偏离轴向。此外，已有的研究集中于光频段，且极少有研究结合两个或多个物理维度实现复用。可见，基于介质超表面在太赫兹频段实现双域或多域多信道复用，同时拓宽介质超表面工作带宽亟待研究。

本文提出一种工作于太赫兹频段的介质超表面，基于该超表面可结合OAM和频率域实现双域多信道复用。当N(N为任意正整数)路具有不同频率和角度的CP平面波沿4个不同方向斜入射至超表面时，在垂

收稿日期：2022-06-17；**修回日期**：2022-07-23；**录用日期**：2022-08-12；**网络首发日期**：2022-08-22
基金项目：湖南省自然科学基金(2022JJ40114)、湖南省教育厅科学研究项目(21C0831)
通信作者：*wangling@hnfnu.edu.cn；**dengl@bupt.edu.cn

直于超表面的方向，$4\times N$路交叉极化透射波都被转换为彼此拓扑正交或频率正交的同轴波束，从而实现$4\times N$路双域多信道复用。超表面基于双域复用法[35]和Pancharatnam-Berry（PB）相位原理（几何相位原理）[36]设计，由介质椭圆柱阵列和介质基板构成。仿真结果表明，对于超表面单元，当入射波为CP波时，交叉极化透射系数的3 dB带宽为0.1 THz，单元工作频段约为0.25～0.35 THz（相对带宽为33.3%）。在该频段内，选取0.25、0.3、0.35 THz三个频点进行仿真验证，基于设计的介质超表面，成功将12路入射波转换为正交同轴波束，即实现了12路信道复用。所提出的介质超表面在高速率大容量太赫兹通信领域具有潜在应用价值。

2 基本原理

为产生拓扑荷为l的OAM波，超表面相位分布φ_l应满足：

$$\varphi_l(x,y)=l\arctan\frac{y}{x},\ l=0,\ \pm1,\ \pm2,\cdots,\tag{1}$$

式中：$(x,\ y)$为超表面上任意坐标位置。

根据广义折射定律和反射定律[37]，设定相位梯度超表面为媒质1和媒质2的分界面，且入射媒质和透射媒质的折射率都为1。当电磁波沿z轴方向从媒质1垂直入射到超表面上时，为实现媒质2中透射波偏转方向的控制，超表面沿x轴和y轴的相位分布φ_d分别可表示为

$$\begin{cases}\varphi_d=\pm\dfrac{2\pi}{D}x\\ \varphi_d=\pm\dfrac{2\pi}{D}y\end{cases},\tag{2}$$

式中：$D=MP$为沿相位梯度方向的超单元周期，P为超表面单元周期，M为组成超单元的单元个数。则透射波沿x轴和y轴的偏转角可表示为

$$\begin{cases}\theta(f)=\arcsin\left(\dfrac{C}{2\pi f}\dfrac{d\varphi_d}{dx}\right)\\ \theta(f)=\arcsin\left(\dfrac{C}{2\pi f}\dfrac{d\varphi_d}{dy}\right)\end{cases},\tag{3}$$

式中：f为频率；C为真空中电磁波的传播速度；$\dfrac{d\varphi_d}{dx}$和$\dfrac{d\varphi_d}{dy}$为相位梯度。基于式（3），对于不同频率的入射波，透射波具有不同的偏转角。

结合式（1）和（2），当一束频率为f的平面波垂直入射至超表面时，为生成4路沿x轴和y轴正负方向偏转、偏转角为$\theta(f)$且携带不同拓扑荷的OAM波束，超表面的传递函数t应满足（忽略生成波束的强度）：

$$t=\sum_{m=1}^{4}\exp\left[j\left(\varphi_{l_m}+\varphi_{d_m}\right)\right]=\exp\left[j\left(l_1\arctan\frac{y}{x}-\frac{2\pi}{D}x\right)\right]+\exp\left[j\left(l_2\arctan\frac{y}{x}-\frac{2\pi}{D}y\right)\right]+\exp\left[j\left(l_3\arctan\frac{y}{x}+\frac{2\pi}{D}x\right)\right]+\exp\left[j\left(l_4\arctan\frac{y}{x}+\frac{2\pi}{D}y\right)\right]。\tag{4}$$

可见，对于不同频率的入射波，基于该超表面都可生成4路携带不同拓扑荷的OAM波束，且频率不同，生成的OAM波束存在不同的偏转角度。

综上所述，超表面相位分布ϕ[35]满足

$$\phi=\mathrm{angle}(t)=\mathrm{angle}\left\{\sum_{m=1}^{4}\exp\left[j\left(\varphi_{l_m}+\varphi_{d_m}\right)\right]\right\},\tag{5}$$

式中：angle{·}表示求解括号中场分布的相位角。当频率为f_n（$n=1,\ 2,\ \cdots,\ N$）的平面波以$\theta_i(f_n)$角度[$\theta_i(f_n)$应满足式（3）]沿$\pm x$轴或$\pm y$轴4个方向斜入射至超表面时，在垂直于超表面的方向上将产生$4\times N$路拓扑正交或频率正交的同轴OAM波。基于此，设计的超表面满足式（5），则为所需的双域复用介质超表面。

值得注意的是，根据式（5）设计的双域复用超表面会存在一些旁瓣。例如：若一束频率为f、与z轴正方向夹角为θ_i、沿x轴负方向入射的平面波$E_i=\exp\left[j(k\sin\theta_i x)\right]$斜入射至超表面，散射场$E_d$可表示为

$$E_d=E_i t=E_{OAM(l_1)}\left(k\sin\theta_i-\frac{2\pi}{D},0\right)+E_{OAM(l_2)}\left(k\sin\theta_i,-\frac{2\pi}{D}\right)+E_{OAM(l_3)}\left(k\sin\theta_i+\frac{2\pi}{D},0\right)+E_{OAM(l_4)}\left(k\sin\theta_i,\frac{2\pi}{D}\right),\tag{6}$$

式中：$k=2\pi/\lambda$，λ为波长；$E_{OAM(l_m)}$（$m=1,2,3,4$）表示拓扑荷为l_m的OAM波束的场分布。根据式（3），$k\sin\theta_i=\dfrac{2\pi}{D}$，$E_d$可表示为

$$E_d=E_{OAM(l_1)}(0,0)+E_{OAM(l_2)}\left(\frac{2\pi}{D},-\frac{2\pi}{D}\right)+E_{OAM(l_3)}\left(\frac{4\pi}{D},0\right)+E_{OAM(l_4)}\left(\frac{2\pi}{D},\frac{2\pi}{D}\right)。\tag{7}$$

可见，在垂直于超表面的方向上产生一束拓扑为 l_1 的 OAM 波束，同时，在 $\left(\frac{2\pi}{D}, -\frac{2\pi}{D}\right)$、$\left(\frac{4\pi}{D}, 0\right)$ 和 $\left(\frac{2\pi}{D}, \frac{2\pi}{D}\right)$ 方向上还会分别产生3束拓扑为 l_2、l_3 和 l_4 的 OAM 波束。

此外，基于PB相位原理[36]，对于超表面单元，当激励为CP波时，透射波由两部分组成：不携带相位偏移的同极化透射波和携带相位偏移的交叉极化透射波。该相位偏移即PB相位，其大小是超表面单元旋转角度的两倍。基于此，可利用PB相位实现所需介质超表面。

3 设计和仿真

3.1 超表面单元设计和仿真

图1为全介质PB超表面基本单元结构示意图，图1(a)、(b)分别为单元结构三维视图和俯视图。单元结构由椭圆形硅(ε=11.9)柱和硅基底构成，周期 P 为 547 μm。椭圆柱短轴 a 的长度为 54 μm，长轴 b 的长度为 540 μm，高度 t_p 为 900 μm，旋转角 φ_{rot} 为长轴与 x 轴正方向的夹角，硅基底厚度 t_s 为 5 μm。

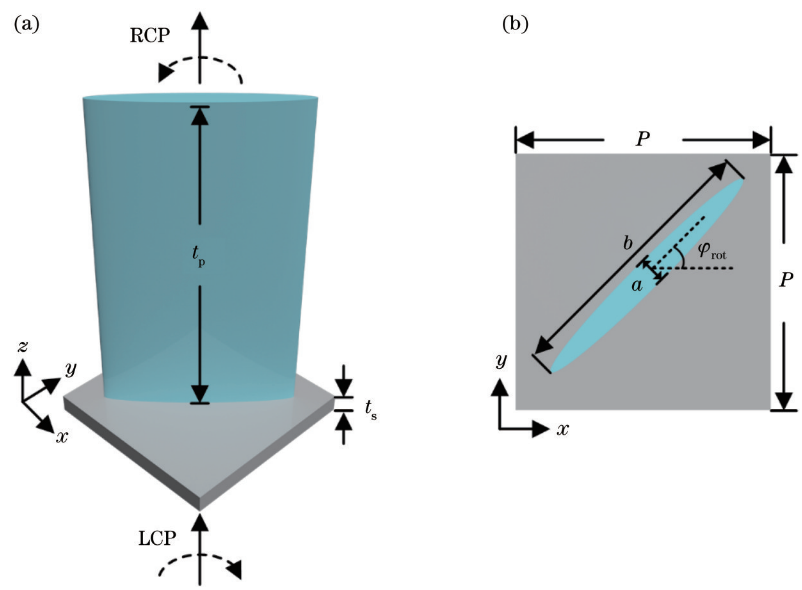

图1 介质单元结构示意图。(a)三维视图；(b)俯视图

Fig. 1 Schematic diagrams of dielectric unit cell. (a) 3D view; (b) top view

基于仿真软件 CST Microwave Studio 对介质单元进行仿真，沿 x 轴和 y 轴方向将单元设置为周期边界，沿 z 轴方向设置上下两个 Floquet 端口，激励设置为沿 z 轴正方向入射的左旋CP(LCP)波。为验证所设计的超表面单元性能，以 φ_{rot} 为0°、30°、70°、120°和180°为例进行仿真(φ_{rot} 可取0°~180°范围内任意值)，右旋CP(RCP)透射系数 T_{RL} 的相位和归一化幅度随频率的变化曲线如图2所示。可见，T_{RL} 的3 dB带宽为 0.1 THz，单元工作频率范围约为0.25~0.35 THz(相对带宽为33.3%)。此外，在该频段，随着 φ_{rot} 从0°变为180°，单元结构可覆盖0°~360°的相位变化。因此，基于PB相位原理，利用该介质单元即可实现所需超表面。

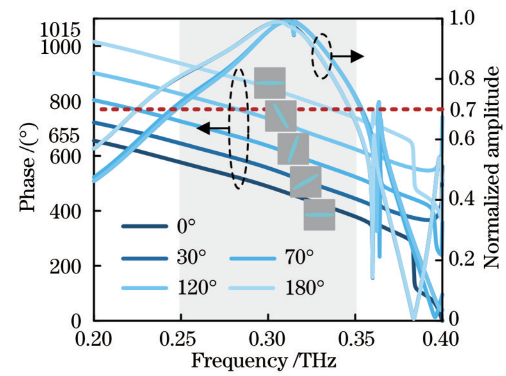

图2 入射波为LCP波，旋转角 φ_{rot} 分别为0°、30°、70°、120°和180°时，单元交叉极化透射系数 T_{RL} 的相位和归一化幅度随频率的变化曲线

Fig. 2 Phase and normalized amplitude of cross-polarized transmission coefficient T_{RL} varying with frequency under LCP incident wave when the rotation angle φ_{rot} is 0°, 30°, 70°, 120°, and 180°, respectively

3.2 超表面设计和仿真

图3为基于太赫兹介质超表面，结合OAM和频率域实现双域多信道复用的示意图。对于通道 C_{11}、C_{21}、C_{31} 和 C_{41}，4路频率为 f_1 且与 z 轴正方向夹角为 $\theta_i(f_1)$ 的 LCP平面波分别沿 $-x$、$-y$、$+x$ 和 $+y$ 方向入射至超表面。在垂直于超表面的方向上，RCP透射波被转换为4路频率为 f_1，拓扑分别为 l_1、l_2、l_3 和 l_4 的同轴波束，即生成了一组频率相同、拓扑正交的同轴波束。同样

地，对于通道 C_{1n}、C_{2n}、C_{3n} 和 C_{4n}，4 路频率为 f_n 且角度为 $\theta_i(f_n)$ 的 LCP 平面波分别沿 $-x$、$-y$、$+x$ 和 $+y$ 方向入射至超表面。在垂直于超表面的方向上，生成一组频率为 f_n 且拓扑正交的同轴波束。最终生成 N 组频率分别为 f_1、f_2、⋯、f_N 且拓扑正交的同轴波束，同时，这 N 组波束彼此的频率正交。可见，$4\times N$ 路斜入射波经过超表面后，在垂直于超表面的方向上都转换为彼此拓扑或频率正交的同轴波束，即结合 OAM 和频率域实现了 $4\times N$ 路双域多信道复用。

为进行仿真验证，本文设定 $l_1=0$、$l_2=-2$、$l_3=+2$、$l_4=-4$ 和 $M=5$，超表面由 14×14 个单元阵列构成。利用式(5)计算出所需介质超表面的相位分布，并基于图 1 中的基本介质单元和 PB 相位原理设计超表面结构。图 4(a)为超表面所需相位分布，图 4(b)为超表面结构三维视图，右下角小图为俯视图。

基于图 2 中超表面单元的性能，以 $f_1=0.35$ THz、$f_2=0.3$ THz、$f_3=0.25$ THz 为例进行仿真验证，并利用式(3)计算出对应的入射角 $\theta_i(f_1)=18.3°$、$\theta_i(f_2)=21.4°$、$\theta_i(f_3)=26°$。根据图 3，对于通道 C_{11}、C_{21}、C_{31} 和 C_{41}，频率为 f_1 的 LCP 平面波分别沿 $-x$、$-y$、$+x$ 和 $+y$ 方向以 $\theta_i(f_1)$ 角度入射至超表面，RCP 透射波远场方向图的幅度和相位仿真结果如图 5 所示。由图 5 可见，通道 C_{11}、C_{21}、C_{31} 和 C_{41} 都在垂直于超表面的方向产生了透射波束。同时，根据 OAM 波束能量和相位分布特点：对于图 5(a)，透射波幅度呈实心分布，相位基本保持不变，因此拓扑荷 $l_1=0$；对于图 5(b)～(d)，透射波

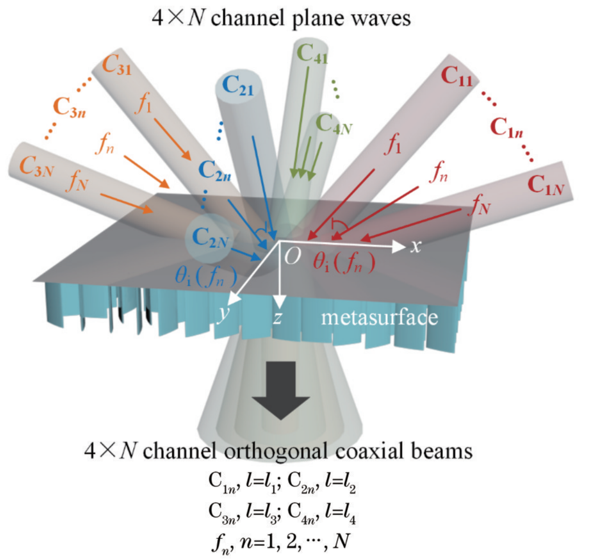

图 3　基于太赫兹介质超表面，结合 OAM 和频率域实现双域多信道复用的示意图

Fig. 3　Schematic diagram of dual-dimensional multi-channel multiplexing based on terahertz dielectric metasurface combined with OAM and frequency

幅度都呈环形分布，相位呈螺旋形分布，且沿 $-z$ 轴方向观察，相位螺旋分别沿顺时针方向改变 4π、-4π 和 8π，即产生了 3 路拓扑荷分别为 $l_2=-2$、$l_3=+2$ 和 $l_4=-4$ 的 OAM 波束。可见，对于通道 C_{11}、C_{21}、C_{31} 和 C_{41}，在垂直于超表面的方向产生了 4 路频率为 f_1、拓扑正交的同轴波束。

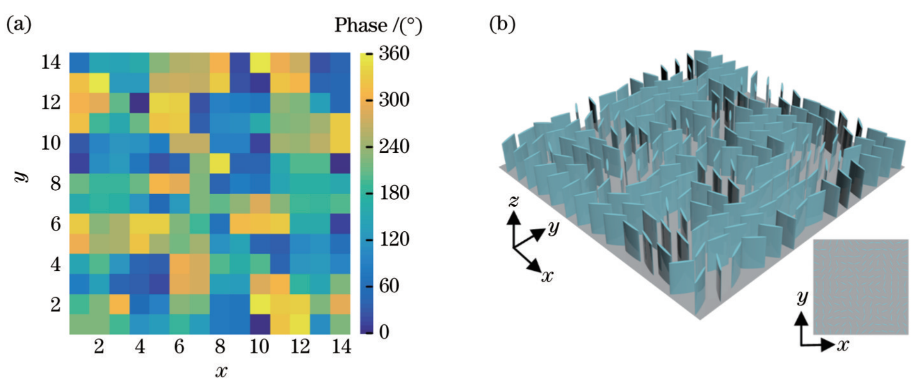

图 4　介质超表面相位分布图和结构示意图。(a)相位分布；(b)三维视图和俯视图

Fig. 4　Schematic diagrams of phase profile and structure of dielectric metasurface. (a) Phase profile; (b) 3D view and top view

同样地，对于通道 C_{12}、C_{22}、C_{32}、C_{42} 和通道 C_{13}、C_{23}、C_{33}、C_{43}，频率为 f_2 和 f_3 的 LCP 平面波分别以角度 $\theta_i(f_2)$ 和 $\theta_i(f_3)$ 沿 $-x$、$-y$、$+x$ 和 $+y$ 方向入射至超表面，RCP 透射波远场方向图的幅度和相位仿真结果如图 6 和图 7 所示。对于通道 C_{12}、C_{22}、C_{32} 和 C_{42}，在垂直于超表面的方向产生了 4 路频率为 f_2 且拓扑正交的同轴波束；对于通道 C_{13}、C_{23}、C_{33} 和 C_{43}，在垂直于超表面的方向产生了 4 路频率为 f_3 且拓扑正交的同轴波束。同时，对于图 5、6 和 7 中产生的 3 组波束，彼此之间频率具有正交性。

综上所述，当 12 路频率分别为 f_1、f_2 和 f_3 的 LCP 平面波以角度 $\theta_i(f_1)$、$\theta_i(f_2)$ 和 $\theta_i(f_3)$ 沿 $-x$、$-y$、$+x$ 和 $+y$ 方向斜入射至超表面，在垂直于超表面的方向上，RCP 透射波都被转换为彼此拓扑正交($l=0,-2,+2,-4$)或频率($f=0.35, 0.3, 0.25$ THz)正交的同轴波束，即结合 OAM 和频率域实现了 12 路双域多信道复用。

此外，以通道 C_{11} 为例，当平面波入射方向为 $(-18.3°, 0°)$ 时，基于式(7)在 $(0, 0)$ 方向上会产生拓

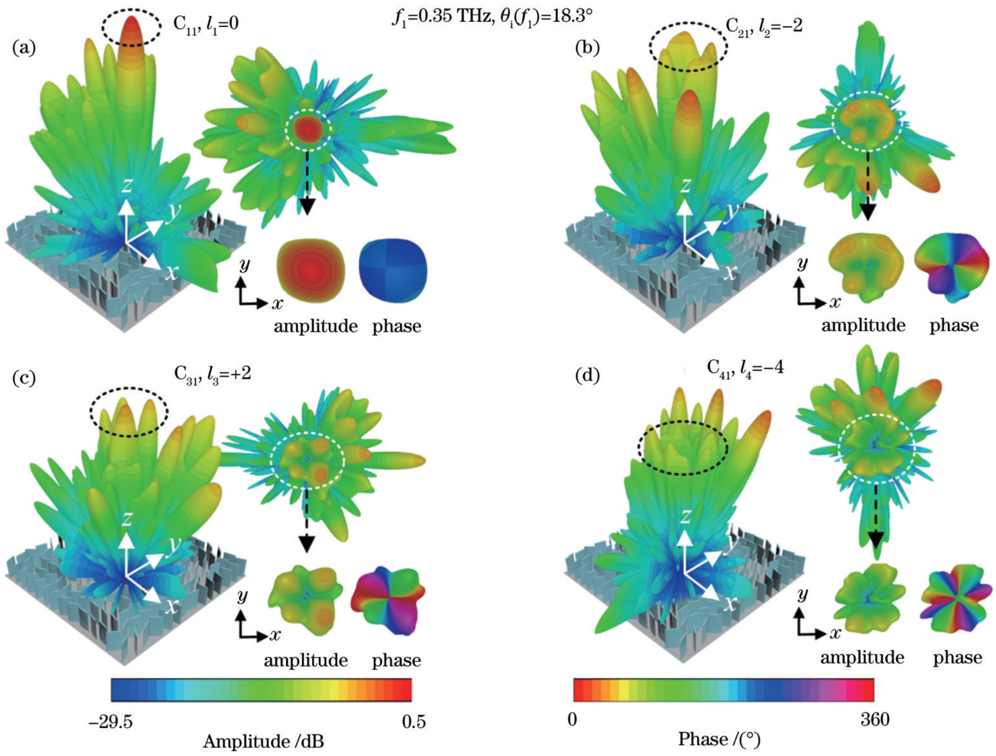

图 5 频率为 f_1 的 LCP 平面波以角度 $\theta_i(f_1)$ 分别沿 $-x$、$-y$、$+x$ 和 $+y$ 方向入射至超表面，RCP 透射波远场方向图的幅度和相位仿真结果。(a)通道 C_{11}；(b)通道 C_{21}；(c)通道 C_{31}；(d)通道 C_{41}

Fig. 5 Simulated far-field amplitude and phase patterns of RCP transmission waves when LCP plane waves with frequency f_1 and angle $\theta_i(f_1)$ are incident on metasurface along with $-x$, $-y$, $+x$, and $+y$ directions, respectively. (a) Channel C_{11}; (b) channel C_{21}; (c) channel C_{31}; (d) channel C_{41}

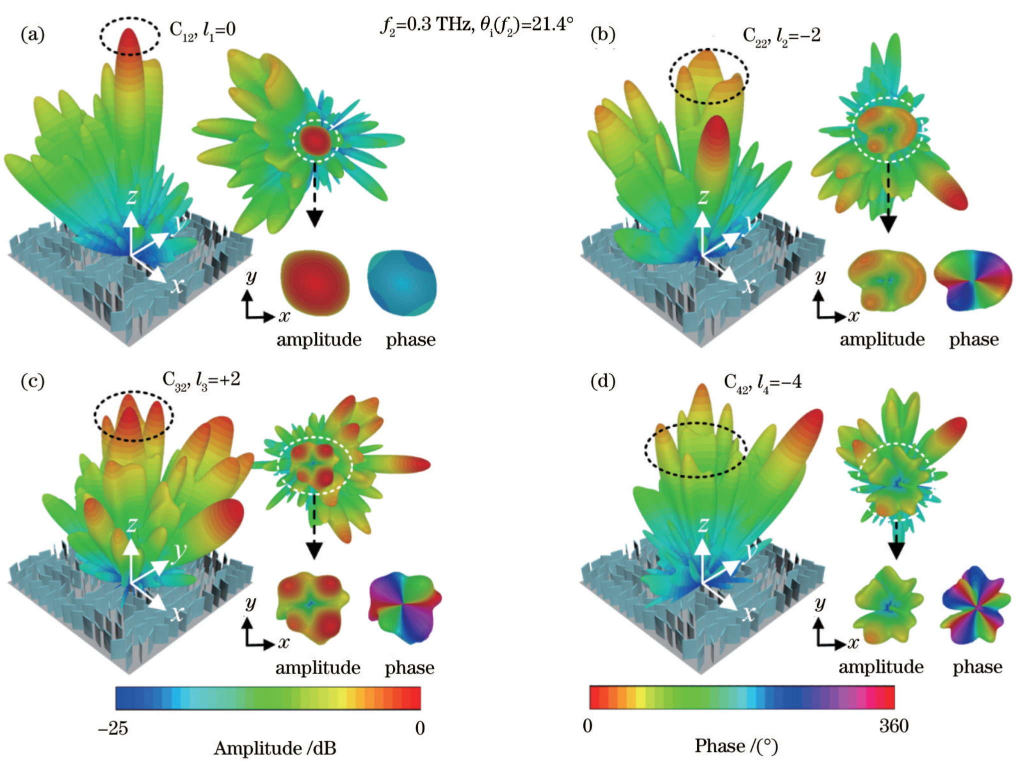

图 6 频率为 f_2 的 LCP 平面波以角度 $\theta_i(f_2)$ 分别沿 $-x$、$-y$、$+x$ 和 $+y$ 方向入射至超表面，RCP 透射波远场方向图的幅度和相位仿真结果。(a)通道 C_{12}；(b)通道 C_{22}；(c)通道 C_{32}；(d)通道 C_{42}

Fig. 6 Simulated far-field amplitude and phase patterns of RCP transmission waves when LCP plane waves with frequency f_2 and angle $\theta_i(f_2)$ are incident on metasurface along with $-x$, $-y$, $+x$, and $+y$ directions, respectively. (a) Channel C_{12}; (b) channel C_{22}; (c) channel C_{32}; (d) channel C_{42}

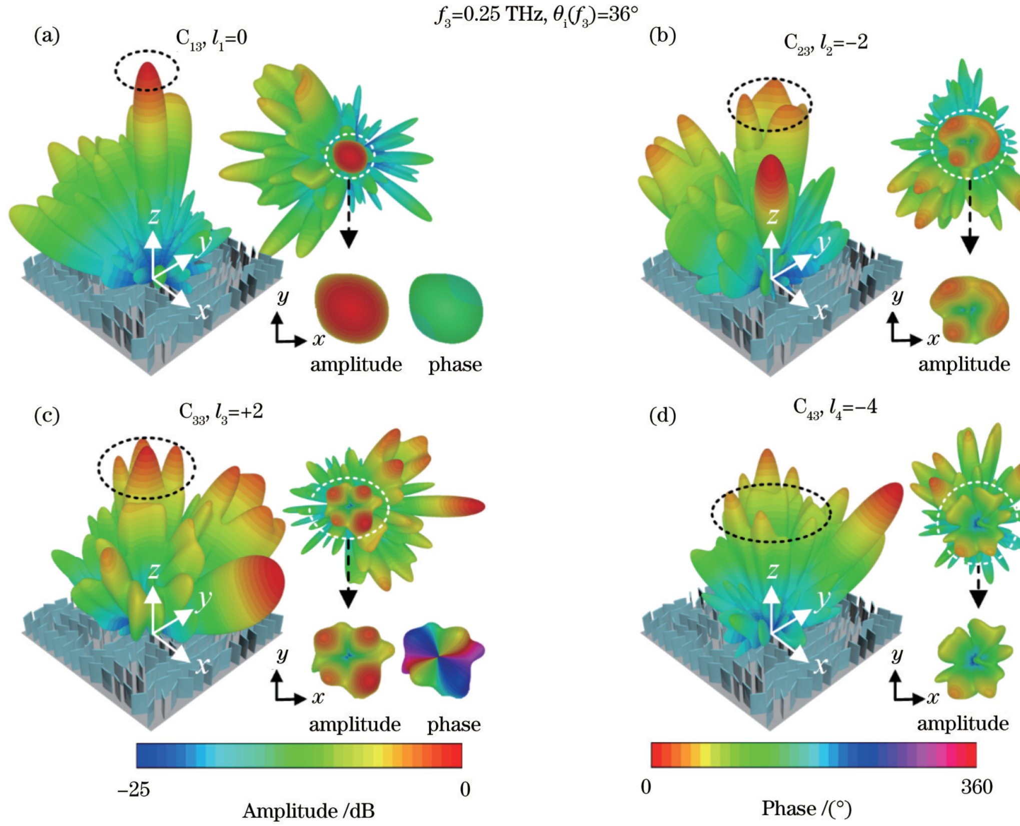

图 7　频率为f_3的 LCP 平面波以角度$\theta_i(f_3)$分别沿$-x$、$-y$、$+x$和$+y$方向入射至超表面，RCP 透射波远场方向图的幅度和相位仿真结果。(a)通道C_{13}；(b)通道C_{23}；(c)通道C_{33}；(d)通道C_{43}

Fig. 7　Simulated far-field amplitude and phase patterns of RCP transmission waves when LCP plane waves with frequency f_3 and angle $\theta_i(f_3)$ are incident on metasurface along with $-x$, $-y$, $+x$, and $+y$ directions, respectively. (a) Channel C_{13}; (b) channel C_{23}; (c) channel C_{33}; (d) channel C_{43}

扑荷为 0 的波束，同时，在约为(−18.3°, 18.3°)、(−36.6°, 0°)和(−18.3°, −18.3°)方向上，还会分别产生拓扑荷为−2、+2 和−4 的 OAM 波束，如图 8 所示。

4　结　　论

本文提出一种工作于 0.25~0.35 THz 的介质超表面，当N路具有不同频率和入射角的 CP 平面波沿 4 个不同方向斜入射至超表面上时，在垂直于超表面的方向上，4×N路交叉极化透射波被转换为彼此拓扑正交或频率正交的同轴波束，即结合 OAM 和频率域实现了 4×N路信道复用。选取f_1=0.35 THz、f_2=0.3 THz 和f_3=0.25 THz 三个频点进行仿真验证。结果表明，当 4 路频率为f_1的 LCP 平面波分别沿$-x$、$-y$、$+x$和$+y$方向以$\theta_i(f_1)$角度斜入射至超表面时，在垂直于超表面的方向产生 4 路频率为f_1且拓扑正交(l=0，−2，+2，−4)的同轴波束。同样地，对于 4 路频率为f_2或f_3、入射角为$\theta_i(f_2)$或$\theta_i(f_3)$的平面波，在垂直于超表面的方向产生 4 路频率为f_2或f_3且拓扑正交的同轴波束。同时，产生的 3 组波束彼此具有频率正交性。可见，基于设计的介质超表面，成功将 12 路入射波转换为彼此拓扑或频率正交的同轴波束，即结合

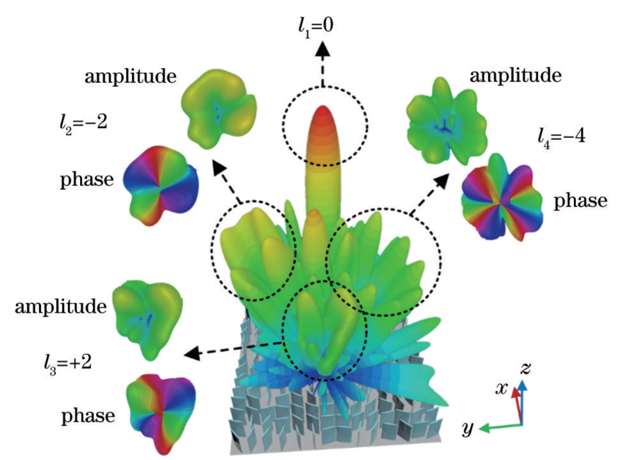

图 8　对于通道C_{11}，当频率为f_1的 LCP 平面波以角度$\theta_i(f_1)$沿$-x$方向即(−18.3°,0°)方向入射至超表面时，RCP 透射波远场仿真结果，以及在约为(−18.3°,18.3°)、(−36.6°,0°)和(−18.3°,−18.3°)方向上的幅度和相位图

Fig. 8　For channel C_{11}, when LCP plane wave with frequency f_1 and angle $\theta_i(f_1)$ is incident on metasurface along with $-x$ direction, that is (−18.3°, 0°), simulated far-field result of RCP transmission wave, and amplitude and phase results in directions of (−18.3°, 18.3°), (−36.6°, 0°), and (−18.3°, −18.3°)

OAM和频率域实现了12路信道复用。此外，基于太赫兹加工测试技术对所设计的超表面进行实验验证[13,38]。所设计的介质超表面在高速率大容量太赫兹通信领域具有潜在的应用价值。

参 考 文 献

[1] Chen Z, Ma X Y, Zhang B, et al. A survey on terahertz communications[J]. China Communications, 2019, 16(2): 1-35.

[2] Winzer P J. Making spatial multiplexing a reality[J]. Nature Photonics, 2014, 8(5): 345-348.

[3] Allen L, Beijersbergen M W, Spreeuw R J C, et al. Orbital angular momentum of light and the transformation of Laguerre-Gaussian laser modes[J]. Physical Review A, 1992, 45(11): 8185-8189.

[4] Bukhari S S, Vardaxoglou J Y, Whittow W. A metasurfaces review: definitions and applications[J]. Applied Sciences, 2019, 9(13): 2727.

[5] Pendry J B, Smith D R. Reversing light with negative refraction [J]. Physics Today, 2004, 57(6): 37-43.

[6] Bai X D, Zhang F L, Sun L, et al. Dynamic millimeter-wave OAM beam generation through programmable metasurface[J]. Nanophotonics, 2022, 11(7): 1389-1399.

[7] Wang Y, Wang H, Su R F, et al. Flexible bilayer terahertz metasurface for the manipulation of orbital angular momentum states[J]. Optics Express, 2021, 29(21): 33445-33455.

[8] 罗蒙. 一种产生涡旋光束的勾型阵列超表面结构设计[J]. 激光与光电子学进展, 2021, 58(1): 0108001.
Luo M. Design of hook-typed metasurface for vortex beams generation[J]. Laser & Optoelectronics Progress, 2021, 58(1): 0108001.

[9] 刘凯婷, 刘鑫, 葛悦禾, 等. 基于高效传输型超表面轨道角动量涡旋波束的产生[J]. 光学学报, 2019, 39(1): 0126016.
Liu K T, Liu X, Ge Y H, et al. Generation of orbital angular momentum vortex beams based on high-efficiency transmission metasurfaces[J]. Acta Optica Sinica, 2019, 39(1): 0126016.

[10] Chen S Q, Xie Z Q, Ye H P, et al. Cylindrical vector beam multiplexer/demultiplexer using off-axis polarization control[J]. Light: Science & Applications, 2021, 10: 222.

[11] 李国强, 施宏宇, 刘康, 等. 基于超表面的多波束多模态太赫兹涡旋波产生[J]. 物理学报, 2021, 70(18): 188701.
Li G Q, Shi H Y, Liu K, et al. Multi-beam multi-mode vortex beams generation based on metasurface in terahertz band[J]. Acta Physica Sinica, 2021, 70(18): 188701.

[12] Yuan Y Y, Zhang K, Ratni B, et al. Independent phase modulation for quadruplex polarization channels enabled by chirality-assisted geometric-phase metasurfaces[J]. Nature Communications, 2020, 11: 4186.

[13] Tan H Y, Deng J H, Zhao R Z, et al. A free-space orbital angular momentum multiplexing communication system based on a metasurface[J]. Laser & Photonics Reviews, 2019, 13(6): 1800278.

[14] 赵静, 王加贤, 赖丽萍, 等. 基于全介质超表面高Q的双带太赫兹传感器[J]. 激光与光电子学进展, 2022, 59(13): 1304004.
Zhao J, Wang J X, Lai L P, et al. High-Q dual-band terahertz sensor based on all-dielectric metasurface[J]. Laser & Optoelectronics Progress, 2022, 59(13): 1304004.

[15] Li C L, Yu P, Huang Y J, et al. Dielectric metasurfaces: from wavefront shaping to quantum platforms[J]. Progress in Surface Science, 2020, 95(2): 100584.

[16] He J N, Wan M L, Zhang X P, et al. Generating ultraviolet perfect vortex beams using a high-efficiency broadband dielectric metasurface[J]. Optics Express, 2022, 30(4): 4806-4816.

[17] Zhou H, Yang J Q, Gao C Q, et al. High-efficiency, broadband all-dielectric transmission metasurface for optical vortex generation[J]. Optical Materials Express, 2019, 9(6): 2699-2707.

[18] Liu Y, Chen L, Zhou C X, et al. Theoretical study on generation of multidimensional focused and vector vortex beams via all-dielectric spin-multiplexed metasurface[J]. Nanomaterials, 2022, 12(4): 580.

[19] Zheng C L, Wang G C, Li J T, et al. All-dielectric metasurface for manipulating the superpositions of orbital angular momentum via spin-decoupling[J]. Advanced Optical Materials, 2021, 9 (10): 2002007.

[20] Li J, Wang G C, Zheng C L, et al. All-silicon metasurfaces for polarization multiplexed generation of terahertz photonic orbital angular momentum superposition states[J]. Journal of Materials Chemistry C, 2021, 9(16): 5478-5485.

[21] Sedeh H B, Salary M M, Mosallaei H. Topological space-time photonic transitions in angular-momentum-biased metasurfaces [J]. Advanced Optical Materials, 2020, 8(11): 2000075.

[22] Ou K, Li G H, Li T X, et al. High efficiency focusing vortex generation and detection with polarization-insensitive dielectric metasurfaces[J]. Nanoscale, 2018, 10(40): 19154-19161.

[23] Liu M Z, Huo P C, Zhu W Q, et al. Broadband generation of perfect Poincaré beams via dielectric spin-multiplexed metasurface[J]. Nature Communications, 2021, 12(1): 2230.

[24] Wang W, Zhao R K, Chang S L, et al. High-efficiency spin-related vortex metalenses[J]. Nanomaterials, 2021, 11(6): 1485.

[25] Xie J F, Guo H M, Zhuang S L, et al. Polarization-controllable perfect vortex beam by a dielectric metasurface[J]. Optics Express, 2021, 29(3): 3081-3089.

[26] Huo P C, Zhang C, Zhu W Q, et al. Photonic spin-multiplexing metasurface for switchable spiral phase contrast imaging[J]. Nano Letters, 2020, 20(4): 2791-2798.

[27] Huo P C, Zhang S, Fan Q B, et al. Photonic spin-controlled generation and transformation of 3D optical polarization topologies enabled by all-dielectric metasurfaces[J]. Nanoscale, 2019, 11(22): 10646-10654.

[28] Mai Q L, Wang C F, Wang X R, et al. Metasurface based optical orbital angular momentum multiplexing for 100 GHz radio over fiber communication[J]. Journal of Lightwave Technology, 2021, 39(19): 6159-6166.

[29] Wang X R, Wang C F, Cheng M L, et al. Broadband structured light multiplexing with dielectric meta-optics[J]. Journal of Lightwave Technology, 2021, 39(9): 2830-2836.

[30] Wang C F, Yang B, Cheng M L, et al. Cylindrical vector beam multiplexing for radio-over-fiber communication with dielectric metasurfaces[J]. Optics Express, 2020, 28(26): 38666-38681.

[31] Du J, Wang J. Dielectric metasurfaces enabling twisted light generation/detection/(de)multiplexing for data information transfer[J]. Optics Express, 2018, 26(10): 13183-13194.

[32] Ha Y L, Guo Y H, Pu M B, et al. Monolithic-integrated multiplexed devices based on metasurface-driven guided waves [J]. Advanced Theory and Simulations, 2021, 4(2): 2000239.

[33] Jin J J, Li X, Pu M B, et al. Angular-multiplexed multichannel optical vortex arrays generators based on geometric metasurface [J]. iScience, 2021, 24(2): 102107.

[34] Li S Q, Li X Y, Zhang L, et al. Efficient optical angular momentum manipulation for compact multiplexing and demultiplexing using a dielectric metasurface[J]. Advanced Optical Materials, 2020, 8(8): 1901666.

[35] Wang L, Yang Y, Deng L, et al. Vanadium dioxide embedded frequency reconfigurable metasurface for multi-dimensional multiplexing of terahertz communication[J]. Journal of Physics D: Applied Physics, 2021, 54(25): 255003.

[36] Bomzon Z, Biener G, Kleiner V, et al. Space-variant Pancharatnam-Berry phase optical elements with computer-generated subwavelength gratings[J]. Optics Letters, 2002, 27 (13): 1141-1143.

[37] Yu N F, Genevet P, Kats M A, et al. Light propagation with phase discontinuities: generalized laws of reflection and refraction

[J]. Science, 2011, 334(6054): 333-337.
[38] Zheng C L, Li J, Wang G C, et al. All-dielectric chiral coding metasurface based on spin-decoupling in terahertz band[J]. Nanophotonics, 2021, 10(4): 1347-1355.

Terahertz Dielectric Metasurface for Dual-Dimensional Multi-Channel Multiplexing

Wang Ling[1*], Gao Feng[1], Teng Shuhua[1], Tan Zhiguo[1], Zhang Xing[1], Lou Jun[1], Deng Li[2**]
[1]*School of Electronic Information, Hunan First Normal University, Changsha* 410205, *Hunan, China*;
[2]*School of Information and Communication Engineering, Beijing University of Posts and Telecommunications, Beijing* 100876, *China*

Abstract

Objective In recent years, the terahertz (THz) band has attracted extensive attention from researchers due to its potential of realizing high-speed and high-capacity wireless communication systems. The multiplexing technology has great research prospects in improving the communication rate and system capacity. The electromagnetic wave (EMW) carrying the orbital angular momentum (OAM) is called the OAM wave. OAM can be used as a new information carrier to provide an additional dimension for spatial multiplexing. The metasurface can effectively control the amplitude, phase, and polarization of EMW, and according to the main types of materials used, it can be divided into the metal and dielectric metasurfaces. Compared with the metal metasurface, the dielectric metasurface has the advantages of smaller ohmic loss, lower costs, easier processing and manufacturing, and higher transmission efficiency. Most previous research focused on generating an OAM beam or realizing OAM beam multiplexing by the metal metasurface, and hence, generating OAM beams and further realizing OAM beam multiplexing based on the dielectric metasurface have become the research hotspots. The methods of OAM beam multiplexing based on the dielectric metasurface have the disadvantages of OAM waves carrying the same information, the limited number of multiplexing channels, and the complexity and high cost of the communication system. Although the above problems can be effectively solved on the basis of the angle-multiplexed dielectric metasurface by converting multiple incident waves with different angles into orthogonal OAM coaxial beams, the current angle-multiplexed dielectric metasurface only works at a single frequency. Once the incident wave frequency changes, the generated OAM waves will deviate from the axis. In addition, the existing research focuses on the optical frequency band, and few studies combine two or more physical dimensions to achieve multiplexing. We need to study the realization of dual-dimensional or multi-dimensional multi-channel multiplexing in the terahertz band based on the dielectric metasurface and the expansion of the working bandwidth of the dielectric metasurface. Therefore, this paper proposes a dielectric metasurface, on the basis of which the dual-dimensional multi-channel multiplexing can be realized by the combination of OAM and frequency dimensions. Theoretically, the simultaneous transmission of $4\times N$-channel (N is any positive integer) orthogonal coaxial beams can be realized. The proposed dielectric metasurface has potential application value in the field of high-speed and high-capacity terahertz communication.

Methods First, the designed dielectric unit cells of the metasurface are composed of silicon pillars and substrates, and unit cells with different rotation angles are simulated on CST Microwave Studio. Periodic boundaries are set in the x-axis and y-axis directions; two Floquet ports are set in the z-axis direction, and the excitation is set as the left circularly polarized (LCP) wave in the negative direction of the z-axis. Then, for topological charges $l_1=0$, $l_2=-2$, $l_3=+2$, and $l_4=-4$, according to the theoretical formula, the required phase distribution of the proposed metasurface is calculated. After that, the metasurface is designed on the basis of the Pancharatnam-Berry (PB) phase principle and the dielectric unit cell. Then, to verify the designed metasurface, we take frequencies $f_1=0.35$ THz, $f_2=0.3$ THz, and $f_3=0.25$ THz to calculate the corresponding incident angle simultaneously. Finally, far-field amplitude and phase patterns of right circularly polarized (RCP) transmission waves are simulated on CST Microwave Studio when three-channel circularly polarized (CP) plane waves with different frequencies and incident angles are obliquely incident on the metasurface in four directions.

Results and Discussions When the rotation angle φ_{rot} of the unit cell is 0°, 30°, 70°, 120°, and 180°, the variations of the simulated phase and normalized amplitude of the cross-polarized transmission coefficient T_{RL} with frequency under LCP incident waves show that the 3 dB bandwidth of T_{RL} of the dielectric unit cell is 0.1 THz, and the working frequency band is about 0.25–0.35 THz (with a relative bandwidth of 33.3%). In addition, as the rotation angle of the unit cell changes

from 0° to 180°, the unit cell can cover the phase change of 0°–360° (Fig. 2). Therefore, the metasurface can be realized on the basis of the PB phase principle and the designed dielectric unit cell. When LCP plane waves with the frequency f_1 and angle $\theta_i(f_1)$ are incident on the metasurface in $\pm x$ and $\pm y$ directions separately, simulated far-field amplitude and phase patterns of RCP transmission waves show that four-channel beams are generated in the direction perpendicular to the metasurface. At the same time, according to the characteristics of OAM beam energy and phase distribution, the amplitude of one of the transmitted waves is in a solid distribution, with the phase unchanged, and thus, the topological charge l_1 equals 0. For the other three-channel beams, the amplitude and phases are distributed in circular and spiral shapes, respectively, and when observed along the $-z$-axis, the phase changes by $+4\pi$, -4π, and $+8\pi$ in a clockwise direction. In other words, the three-channel OAM beams with topological charges of $l_2=-2$, $l_3=+2$, and $l_4=-4$ are generated. It can be seen that four-channel topologically orthogonal coaxial beams with frequency f_1 are generated in the direction perpendicular to the metasurface (Fig. 5). Similarly, for four-channel LCP plane waves with f_2 and $\theta_i(f_1)$, or f_3 and $\theta_i(f_3)$ incident on the metasurface along the $\pm x$ and $\pm y$ axes, four topologically orthogonal coaxial beams with frequency f_2 or f_3 in the direction perpendicular to the metasurface are generated (Figs. 6 and 7).

Conclusions In this paper, a dielectric metasurface working at 0.25–0.35 THz is proposed. When N-channel CP plane waves with different frequencies and incident angles are obliquely incident on the metasurface in four directions, in the direction perpendicular to the metasurface, $4\times N$-channel cross-polarized transmission waves are converted into coaxial beams that are orthogonal to each other in topology or frequency, namely that the $4\times N$ channel multiplexing is realized. For simulation verification, we assume $f_1=0.35$ THz, $f_2=0.3$ THz, and $f_3=0.25$ THz. The simulations show that when four-channel LCP plane waves with frequency f_1, f_2, or f_3 are obliquely incident on the metasurface along the $\pm x$ and $\pm y$ axes, four topologically orthogonal coaxial beams with frequency f_1, f_2, or f_3 in the direction perpendicular to the metasurface are generated. At the same time, the generated three groups of beams are orthogonal to each other in frequency. It can be seen that on the basis of the designed dielectric metasurface, 12-channel incident waves are successfully converted into coaxial beams with topology or frequency orthogonality. In other words, 12-channel multiplexing is realized by the combination of OAM and frequency dimensions. The designed dielectric metasurface has potential application value in the field of high-speed high-capacity terahertz communication.

Key words optics at surfaces; terahertz; dielectric metasurface; multiplexing; orbital angular momentum